

热处理对激光选区熔化成形 TC11 钛合金组织性能的影响

窦恩惠*, 肖美立, 柯林达, 杜磊, 赖彩芳

上海航天精密机械研究所, 上海 201600

摘要 研究了退火温度和保温时间对激光选区熔化(SLM)成形 TC11 钛合金组织性能及断裂机制的影响。结果表明:SLM 成形 TC11 钛合金沉积态的组织为针状马氏体,显微硬度为 402 HV_{0.5},抗拉强度和断后伸长率分别为 1557 MPa 和 2.5%,表现出高强度、低塑性的特点。经 850 °C/4 h 和 950 °C/4 h 退火后,组织分别为细密的 $\alpha+\beta$ 混合组织和 $\alpha+\beta$ 网篮组织,硬度和强度降低,断后伸长率升高;且断裂模式由沿晶断裂转变为韧性断裂,这与断后伸长率的变化规律一致。经 950 °C 退火后,随退火时间缩短, α 片层越细密,且晶界 α 相由连续分布转变为非连续分布,导致抗拉强度和断后伸长率同时增加。经 950 °C/1 h 退火后,可获得强度和塑性匹配较佳的 TC11 钛合金,其抗拉强度和断后伸长率分别为 1051 MPa 和 19.8%。

关键词 激光技术;激光选区熔化;TC11 钛合金;热处理;组织性能;断裂机制

中图分类号 TG166.5

文献标志码 A

doi: 10.3788/CJL202148.0602117

1 引言

TC11 钛合金作为一种 $\alpha+\beta$ 型钛合金,其比刚度、比强度、耐腐蚀性、抗蠕变性及热稳定性好,且在 500 °C 以下具有较高的强度,在航空航天领域得到广泛的应用^[1-4]。但采用传统“锻造+机加”的技术制造航空航天复杂精密零部件时,面临工序繁杂、工艺困难、材料利用率低等问题,制约了国防装备的发展^[5-6]。

增材制造技术无疑可以解决传统加工面临的难题^[7]。目前,关于 TC11 钛合金的增材制造的研究主要集中于激光熔化沉积(LMD)成形^[8-10],但 LMD 在成形复杂精密零件时具有局限性。而激光选区熔化(SLM)作为另一种激光快速成形技术,成形精度高于 LMD,可实现难加工材料和复杂精密零部件的直接制造^[11]。

SLM 制备的金属材料的力学性能具有各向异性、高强度低塑性的特点^[12-13],通常需要热处理来调控组织,进而使其满足使用要求。目前,有关 SLM 成形 TC11 钛合金热处理的研究鲜有报道,

而 TC11 与 TC4 都是 $\alpha+\beta$ 型钛合金,因此 SLM 成形 TC4 钛合金的热处理工艺具有一定参考意义。肖振楠等^[14]研究了退火、固溶、固溶时效对 SLM 成形 TC4 钛合金组织性能的影响,结果表明,退火后可获得较佳强度和塑性匹配的钛合金。张伟祥等^[15]研究了退火温度对 SLM 成形 TC4 钛合金组织性能的影响,结果表明,800 °C 退火时,可以完全消除马氏体,且保温 2 h 炉冷后,其综合力学性能最佳。Vrancken 等^[16]研究了 SLM 成形 TC4 钛合金在热处理后的组织性能,850 °C/2 h 后炉冷,试样的断后伸长率由 7.36% 提高至 12.84%。退火可以使 SLM 成形钛合金获得优良的力学性能。因此,研究退火温度和保温时间对 SLM 成形钛合金组织性能和断裂机制的影响规律具有重要意义。本实验采用 SLM 成形 TC11 钛合金,对比研究不同加热温度和保温时间下的显微组织、力学性能和断口形貌,深入探究不同状态下的断裂机制,为进一步调控 SLM 成形钛合金的组织性能提供一定参考,并为工程应用提供依据。

收稿日期: 2020-06-23; 修回日期: 2020-08-04; 录用日期: 2020-10-14

* E-mail: douenhui@126.com

2 试验材料及方法

试验材料为气雾化法制备的 TC11 钛合金球形粉末,通过机械筛分获得粒径为 15~53 μm 的颗

表 1 TC11 钛合金粉末化学成分

Table 1 Chemical compositions of TC11 titanium alloy powder

Element	Ti	Al	Mo	Zr	Si	Fe	C	N	H	O
Mass fraction /%	Bal.	6.380	3.460	1.680	0.246	0.017	0.080	0.007	0.006	0.120

采用新瑞达 NRD-SLM-300A 成形设备,最大成形尺寸为 250 mm \times 250 mm \times 300 mm,单层最小铺粉厚度为 20 μm 。激光器为德国 IPG 生产的 500 W 光纤激光器,采用振镜式扫描方式,最大扫描速度为 7000 mm/s。实验过程中通入高纯氩气。成形过程如图 1 所示。采用的工艺参数:激光功率为 425 W,扫描速度为 1000 mm/s,扫描间距为 0.15 mm,层厚为 0.06 mm。退火温度和时间参照 GB/T 37584-2019《钛及钛合金制件热处理》,保温一定时间后,随炉冷却(FC),具体热处理工艺参数如表 2 所示。

表 2 SLM 成形 TC11 钛合金热处理工艺

Table 2 Heat treatment process for TC11 titanium alloys formed by SLM

Heat treatment mode	Heat treatment condition
Annealing	850 $^{\circ}\text{C}$ /4 h/FC
Annealing	950 $^{\circ}\text{C}$ /4 h/FC
Annealing	950 $^{\circ}\text{C}$ /2 h/FC
Annealing	950 $^{\circ}\text{C}$ /1 h/FC

采用 D8 Advanced X 射线衍射仪(XRD)对打磨及抛光后的 YZ 表面进行物相分析,扫描范围为 30 $^{\circ}$ ~80 $^{\circ}$,扫描速度为 10 ($^{\circ}$)/min。采用 Kroll 试剂腐蚀试样后,在 LEICA DMR 金相(OM)显微镜和 FEI QUANTA 450 扫描电镜(SEM)下观察组织。采用华银 HVS-1000A 显微维氏硬度计测试硬度,测试位置如图 1 所示。距离试样上表面 2 mm,测量 5 个点的显微硬度,取其平均值。测量间距为 0.5 mm,载荷为 4.90 N,保荷 15 s。采用美斯特 XYA 105C 型微机控制电子万能试验机测试室温拉伸性能,拉伸速率为 2 mm/min,拉伸试样参照 GB/T 228.1-2010《金属材料 拉伸试验 第 1 部分:室温试验方法》,试样尺寸如图 2 所示,并采用 SEM 观察断口形貌。

粒,其名义化学成分如表 1 所示。使用前将粉末材料烘干 4~8 h。基板选用 45 mm 厚的 TC4 钛合金,表面经吹砂处理后,用酒精擦拭干净。

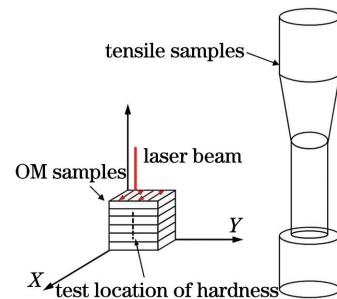


图 1 SLM 成形示意图

Fig. 1 Schematic of SLM forming

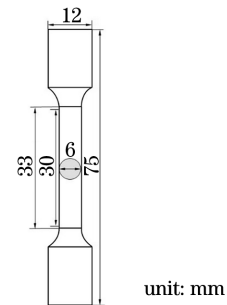


图 2 SLM 成形 TC11 钛合金拉伸件

Fig. 2 Tensile part of TC11 titanium alloy formed by SLM

3 分析与讨论

3.1 组织特征

图 3 是 SLM 成形 TC11 钛合金的 XRD 图。可

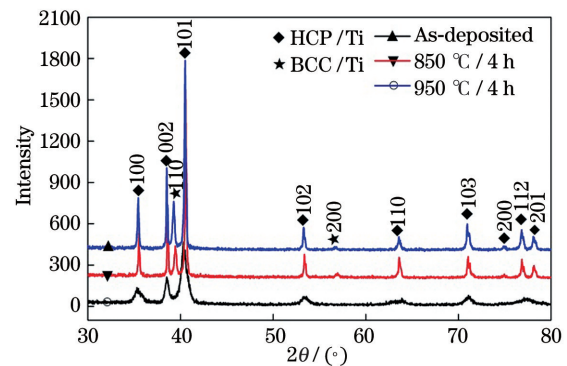


图 3 SLM 成形 TC11 钛合金的 XRD 图

Fig. 3 XRD pattern of TC11 titanium alloys formed by SLM

知,退火态中密排六方 Ti(HCP/Ti)的衍射峰位置与沉积态中的相似,且沉积态中不存在体心立方 Ti(BCC/Ti)的衍射峰。表明沉积态试样由 HCP/Ti 组成,而退火态试样由 HCP/Ti 和 BCC/Ti 组成。通过点阵常数的计算可知,沉积态中 HCP/Ti 的 a 和 c 分别为 0.2934 nm 和 0.46757 nm,结果与 α' 相一致^[17];退火态中 HCP/Ti 的 a 和 c 分别为 0.29172 nm 和 0.46817 nm,结果与 α 相一致^[18]。

图 4 是 SLM 成形 TC11 钛合金沉积态的组织

形貌。可以观察到,宏观组织呈柱状晶形貌,晶粒的宽度为 60~120 μm ,长度为 0.6~1.6 mm。细长的原始初生 β 晶粒穿过数十沉积层,表现出外延生长的取向,如图 4(a)所示。与 LMD 制备的 TC11 钛合金相比,SLM 成形 TC11 钛合金的柱状晶明显细小^[9]。晶粒内部均匀分布细针状组织,如图 4(b)、(c)所示。结合图 3 的结果可知,针状组织为 α' 马氏体,这也是 SLM 成形 TC4 钛合金的典型组织^[14,19]。

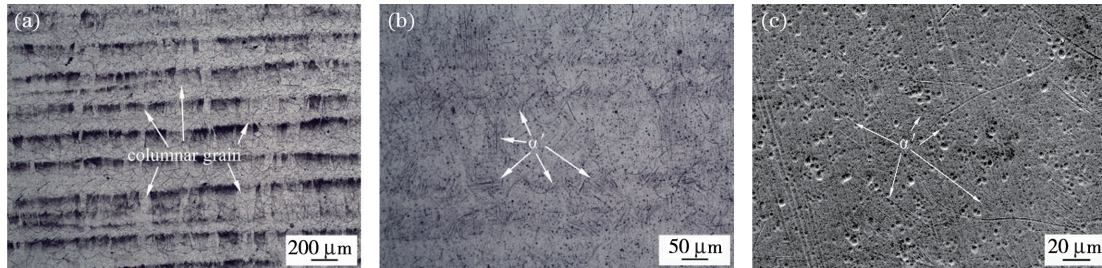


图 4 SLM 成形 TC11 钛合金沉积态的组织形貌。(a)宏观形貌;(b)OM 微观组织;(c)微观组织的 SEM

Fig. 4 Microstructure of deposited TC11 titanium alloy formed by SLM. (a) Macro morphology; (b) OM of microstructure; (c) SEM of microstructure

在 SLM 成形过程中,晶粒顶部发生重熔,重熔晶粒表面为现成的形核质点,且沿着沉积方向的散热速度最快,因此晶粒逆着散热方向发生外延生长,形成柱状晶组织^[20]。其晶粒尺寸细小,是因为 SLM 成形过程中熔池更小,液态停留时间更短和冷却速率更快,故生成较小的柱状晶^[21]。而工艺过程中的冷却速率是晶粒内部微观组织的主要影响因

素^[13],有研究表明^[22],SLM 成形技术的冷却速率高达 $10^8 \text{ K} \cdot \text{s}^{-1}$,快速冷却导致 β 相发生马氏体转变,形成细针状 α' 马氏体。

图 5 为 SLM 成形 TC11 钛合金在不同加热温度下的组织形貌。结合图 3 结果可知:在 850 $^{\circ}\text{C}$ / 4 h 条件下,微观组织由细密的 $\alpha + \beta$ 混合组织构成。针状 α 宽度约为 0.5 μm ,这是一种亚稳 α' 相形

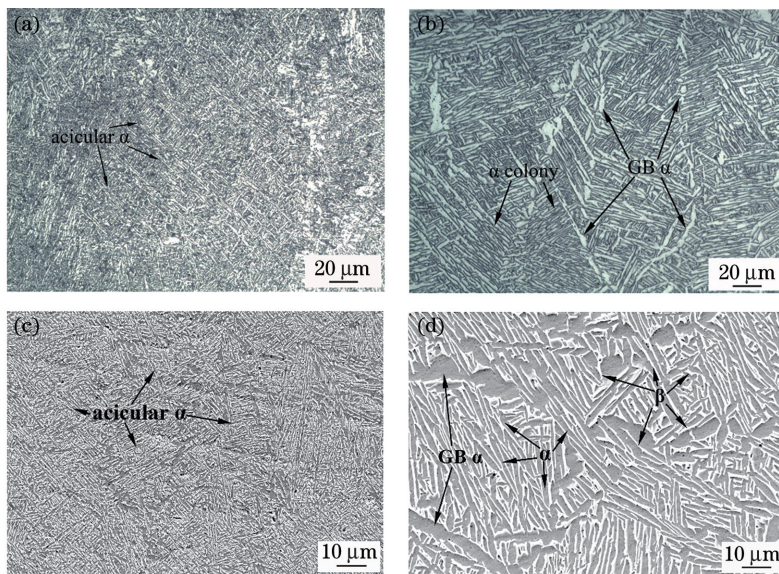


图 5 SLM 成形 TC11 钛合金在不同加热温度下的组织形貌。(a)850 $^{\circ}\text{C}$ / 4 h 条件下的 OM 图;(b)950 $^{\circ}\text{C}$ / 4 h 条件下的 OM 图;(c)850 $^{\circ}\text{C}$ / 4 h 条件下的 SEM 图;(d)950 $^{\circ}\text{C}$ / 4 h 条件下的 SEM 图

Fig. 5 Microstructure of TC11 titanium alloy formed by SLM under different heating temperature. (a) OM image at 850 $^{\circ}\text{C}$ / 4 h; (b) OM image at 950 $^{\circ}\text{C}$ / 4 h; (c) SEM image at 850 $^{\circ}\text{C}$ / 4 h; (c) SEM image at 950 $^{\circ}\text{C}$ / 4 h

核和长大,分解形成 $\alpha+\beta$ 的稳定组织;在 $950\text{ }^{\circ}\text{C}/4\text{ h}$ 条件下,组织呈现出网篮组织形貌,由片层状的 $\alpha+\beta$ 相组成。 α 相的片层宽度为 $2\sim 5\text{ }\mu\text{m}$,且在晶粒内部和晶界处分别形成 α 集束和连续的晶界 α 相(GB α)。结果表明,保温时间相同,加热温度不同时,SLM 成形 TC11 钛合金退火组织形貌不同。退火温度增加,原子扩散充分, α 相的片层粗化并发生积聚,形成取向相同的 α 集束,有的 α 集束甚至贯穿整个晶粒。

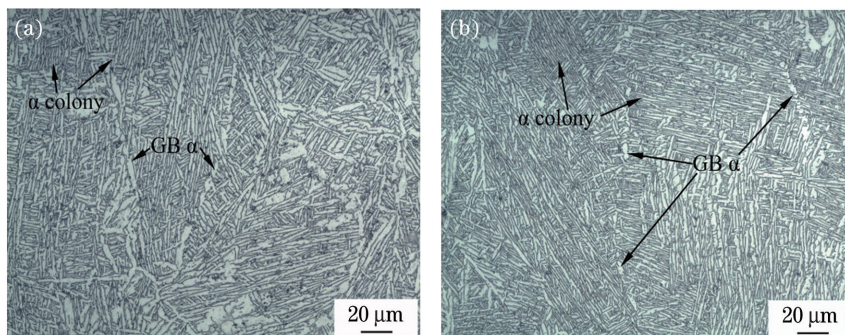


图 6 SLM 成形 TC11 钛合金在不同保温时间下的组织形貌。(a) $950\text{ }^{\circ}\text{C}/2\text{ h}$; (b) $950\text{ }^{\circ}\text{C}/1\text{ h}$

Fig. 6 Microstructure of TC11 titanium alloy formed by SLM under different holding time. (a) $950\text{ }^{\circ}\text{C}/2\text{ h}$; (b) $950\text{ }^{\circ}\text{C}/1\text{ h}$

$950\text{ }^{\circ}\text{C}$ 退火时,GB α 相可能是截止在 β 晶界的针状 α' 相分解形成 $\alpha+\beta$ 相后, α 相长大的结果。在保温及随后的缓冷过程中,GB α 相更容易沿着晶界继续长大。因为 GB α 相通常选择性形核和长大,即在晶界的缺陷和高能位置形核^[23]。当保温时间较长时,GB α 相合并成连续分布的相,而保温时间较短时,GB α 相并未接触,因此呈非连续分布。

3.2 显微硬度

图 7 为 SLM 成形 TC11 钛合金的显微硬度变化趋势。可知,沉积态的 TC11 钛合金的平均显微硬度为 $402\text{ HV}_{0.5}$, $950\text{ }^{\circ}\text{C}/4\text{ h}$ 条件下的显微硬度为

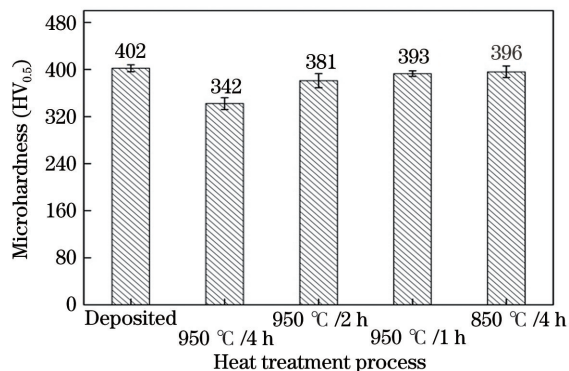


图 7 不同热处理工艺下 SLM 成形 TC11 钛合金的显微硬度

Fig. 7 Microhardness of TC11 titanium alloy formed by SLM under different heat treatment process

图 6 为 SLM 成形 TC11 钛合金在不同保温时间下的组织形貌。可知,在 $950\text{ }^{\circ}\text{C}$,分别保温 2 h 和 1 h 条件下,组织均形成网篮形貌,但 α 相片层宽度不同,分别为 $1\sim 2\text{ }\mu\text{m}$ 和 $0.5\sim 1\text{ }\mu\text{m}$,约为 $950\text{ }^{\circ}\text{C}/4\text{ h}$ 条件下的 $1/2$ 和 $1/4$ 。此外,GB α 相开始转变为非连续分布。结果表明,加热温度相同,保温时间不同时,SLM 成形 TC11 钛合金退火组织形貌相同。但是随着保温时间的缩短, α 片层更加细小,且 GB α 相减少,并由连续分布转变为非连续分布。

$342\text{ HV}_{0.5}$,仅为沉积态的 85% ,降低显著。同样保温 4 h , $850\text{ }^{\circ}\text{C}$ 条件下的显微硬度为 $396\text{ HV}_{0.5}$,下降却不明显。而在 $950\text{ }^{\circ}\text{C}$,分别保温 2 h 和 1 h 条件下,显微硬度分别为 $381\text{ HV}_{0.5}$ 和 $393\text{ HV}_{0.5}$,比 $950\text{ }^{\circ}\text{C}/4\text{ h}$ 条件下的有明显升高。

以上结果表明,SLM 成形 TC11 钛合金显微硬度的变化规律与组织的演变规律是一致的。马氏体 α' 是 β 晶粒通过非扩散的方式形成的,溶质原子的含量与 β 相似,其晶格畸变能高,固溶强化作用明显。 $950\text{ }^{\circ}\text{C}/4\text{ h}$ 条件下退火时,原子发生扩散, α' 马氏体分解,并形成粗大的 $\alpha+\beta$ 网篮组织,晶格畸变减弱,导致材料软化,硬度损失严重;但随着保温时间减少,形成的 α 片层越细小, α/β 的相界面越多,反而具有细晶强化的作用,因此硬度随保温时间减少而增加。与 $950\text{ }^{\circ}\text{C}$ 退火下的硬度相比, $850\text{ }^{\circ}\text{C}/4\text{ h}$ 条件下更易形成更细密的 $\alpha+\beta$ 组织,导致硬度值相对较高。

3.3 拉伸性能

SLM 成形 TC11 钛合金的拉伸性能如表 3 所示,其应力-应变曲线如图 8 所示。沉积态的抗拉强度和断后伸长率分别为 1557 MPa 和 2.5% ,表现出高强度、低塑性的特点。因为 SLM 成形 TC11 钛合金晶粒内形成大量细针状马氏体,这种组织的特点就是强度高,塑性差。 $850\text{ }^{\circ}\text{C}/4\text{ h}$ 和 $950\text{ }^{\circ}\text{C}/4\text{ h}$ 条

表 3 不同热处理工艺下 SLM 成形 TC11 钛合金力学性能
Table 3 Mechanical properties of TC11 titanium alloy formed by SLM under different heat treatment process

Heat treatment process	Tensile strength /MPa	Elongation /%
Deposited	1557±29	2.5±1
850 °C /4 h	1121±14	11.8±1.8
950 °C /4 h	996±5	14.3±3
950 °C /2 h	1040±2	16±0.5
950 °C /1 h	1051±2	19.8±0.7

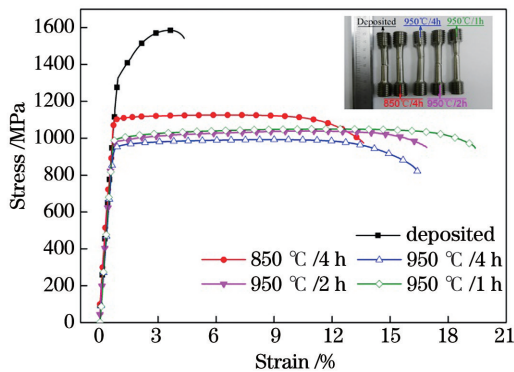


图 8 不同热处理工艺下 SLM 成形 TC11 钛合金的应力-应变曲线

Fig. 8 Stress-strain curves of TC11 titanium alloy formed by SLM under different heat treatment process

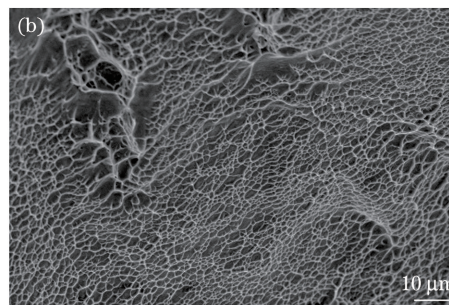
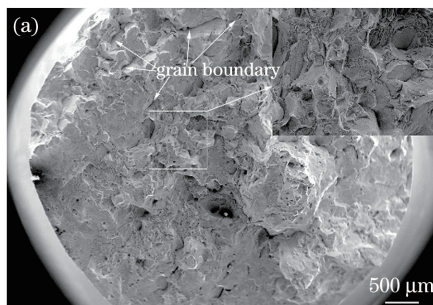


图 9 沉积态的断口形貌。(a)宏观断口;(b)微观断口

Fig. 9 Fracture morphologies of deposited samples. (a) Macro fracture; (b) micro fracture

图 9(b)为沉积态的微观断口形貌,可知,沉积态的微观断口表现出撕裂的韧窝特征,韧窝尺寸为 $1\sim 2\ \mu\text{m}$,且韧窝较浅,呈现出沿晶韧窝断口的特征。因为沉积态的组织为马氏体 α' ,塑性变形能力相对较差,且柱状晶的晶界一般处于高能状态,抵抗裂纹扩展的抗力较低。在外载荷的作用下,裂纹在晶界或者内部缺陷处萌生,并且沿晶界扩展,形成沿晶界的韧窝断口。所以在室温拉伸时,沉积态的 TC11 钛合金发生沿晶断裂。

图 10 为退火态的断口形貌,发现退火态的宏观断口均存在明显的塑性变形。断裂时发生颈缩,表

件下的抗拉强度分别为 1121 MPa 和 996 MPa,约为沉积态的 72% 和 64%,而断后伸长率分别为 11.8% 和 14.3%,约为沉积态的 4.5 倍和 5.7 倍。表明 SLM 成形 TC11 钛合金经退火后的强度显著降低,塑性大幅提高。因为马氏体组织的转变,强度降低,塑性提高。

此外,退火温度(950 °C)相同时,随着退火时间的减少,不仅抗拉强度由 996 MPa 增加至 1050 MPa,而且断后伸长率也由 14.3% 增加至 19.8%。一方面,因为网篮组织越细密,其包含的 α/β 相界面越多,增大了位错运动阻力,起到细晶强化的作用;另一方面,塑性提高与 GB α 相有关^[9,24]。 α 相为密排六方结构,塑性变形能力差。GB α 相连续分布时,对位错的阻力较大;非连续分布时,位错可以绕过 GB α 相,滑移到邻近晶粒,并进一步在邻近晶粒内滑移。因此,网篮组织越细密,GB α 相越少,强度越高,塑性得到改善。

3.4 断裂机制

图 9 为 SLM 成形 TC11 钛合金沉积态的室温拉伸断口。可以观察到,宏观断口没有明显的塑性变形,且断口表现出不同位向的颗粒状的晶粒表面,同时存在开裂的晶界,如图 9(a)所示,这是裂纹沿晶界扩展的结果。

现出“杯锥状”的特征;断口表面存在明显的纤维区和放射区,这是塑性断裂的特征,如图 10(a)所示。但是在 850 °C/4 h 条件下的断口纤维区内,仍然可以观察到部分具有立体感的晶粒,如图 10(a)第 1 张图所示。结果表明,850 °C/4 h 条件下的试样也有可能存在沿晶断裂。

图 10(b)为退火态样品的微观断口形貌,均表现出等轴韧窝的特征。可知,850 °C/4 h 条件下的韧窝尺寸与沉积态的相当,但比沉积态的深。此外,850 °C/4 h 条件下的断口存在晶粒表面的撕裂棱和二次裂纹,这些二次裂纹同样是晶界开裂的结果,如

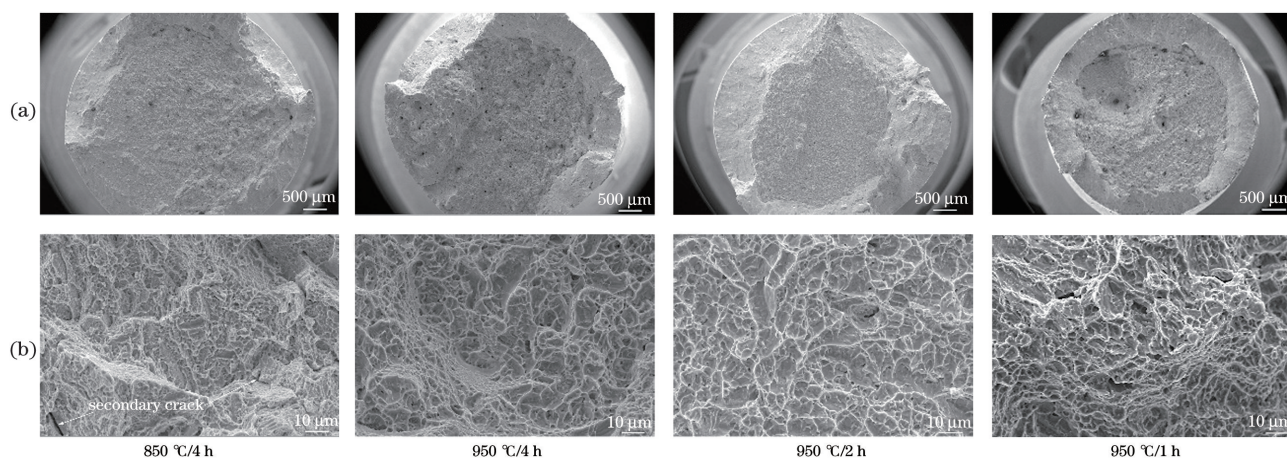


图 10 退火态样品的断口形貌。(a)宏观断口;(b)微观断口

Fig. 10 Fracture morphologies of annealed samples. (a) Macro fracture; (b) micro fracture

图 10(b)第 1 张图所示。结果表明,850 °C/4 h 条件下的试样在室温拉伸时,其断裂模式是沿晶断裂和韧性断裂的混合断裂模式,这也是 850 °C/4 h 条件下断后伸长率高于沉积态的原因。

950 °C/4 h 条件下,试样的微观断口表面存在大量的韧窝和塑性撕裂棱,韧窝尺寸为 5~10 μm ,约为 850 °C/4 h 条件下的 5 倍,且韧窝较深,如图 10(b)第 2 张图所示。950 °C/2 h 和 950 °C/1 h 条件下的微观断口形貌与 950 °C/4 h 条件下的一致,并且韧窝的尺寸相当,如图 10(b)第 3 张图和第 4 张图所示,表明 SLM 成形 TC11 钛合金经过 950 °C 退火后,试样在室温拉伸下发生韧性断裂。以上结果表明,断口形貌的变化特征与断后伸长率的变化规律一致,且退火温度对断口的微观形貌影响显著,退火时间的影响较小。

4 结 论

采用 SLM 成形 TC11 钛合金,通过微观组织、显微硬度、拉伸性能及断口分析,研究了退火温度与时间对其组织性能和断裂机制的影响。SLM 成形 TC11 钛合金沉积态的宏观组织为沿沉积方向优先生长的柱状晶,晶粒内形成细针状马氏体组织。经 850 °C/4 h 和 950 °C/4 h 退火后,分别形成细密的 $\alpha+\beta$ 混合组织和 $\alpha+\beta$ 网篮组织,且随着退火时间的缩短, $\alpha+\beta$ 网篮组织逐渐细化,GB α 相也逐渐减少。SLM 成形 TC11 钛合金沉积态的显微硬度约为 402 HV_{0.5}。经过 950 °C/4 h 退火后, $\alpha+\beta$ 网篮组织粗化,导致 SLM 成形 TC11 钛合金软化,显微硬度约为沉积态的 85%,且随着退火时间或温度的降低,显微硬度逐渐升高。SLM 成形 TC11 钛合金

沉积态的抗拉强度和断后伸长率分别为 1557 MPa 和 2.5%;退火态的强度为 996~1121 MPa,断后伸长率为 11.8%~19.8%,其强度降低,塑性提高。且经 950 °C 退火时,随着退火时间缩短,其强度和塑性均提高,950 °C/1 h 条件下可获得强度和塑性的最佳匹配。

在室温拉伸的条件下,沉积态的 SLM 成形 TC11 钛合金发生沿晶断裂,经 850 °C/4 h 退火后的试样发生沿晶和韧性的混合断裂,经 950 °C 退火后的试样发生韧性断裂。

参 考 文 献

- [1] Zhao W Q, Chen J, Yang J Q, et al. Influences of laser solid forming process on microstructure and mechanical properties of TC11 titanium alloy [J]. Applied Laser, 2012, 32(6): 479-483.
赵卫强, 陈静, 杨杰穷, 等. 激光立体成形工艺对 TC11 钛合金组织和力学性能的影响[J]. 应用激光, 2012, 32(6): 479-483.
- [2] Cui C X, Hu B M, Zhao L C, et al. Titanium alloy production technology, market prospects and industry development [J]. Materials & Design, 2011, 32(3): 1684-1691.
- [3] Lei L M, Huang X, Wang M M, et al. Effect of temperature on deformation behavior and microstructures of TC11 titanium alloy [J]. Materials Science and Engineering: A, 2011, 528(28): 8236-8243.
- [4] Li Z, Li J, Liu J, et al. Structure and formation mechanism of α/α interface in laser melting deposited $\alpha+\beta$ titanium alloy [J]. Journal of Alloys and Compounds, 2016, 657: 278-285.
- [5] Chen X J, Zhao G R, Dong D D, et al. Microstructure and mechanical properties of

- Inconel625 superalloy fabricated by selective laser melting [J]. Chinese Journal of Lasers, 2019, 46 (12): 1202002.
- 陈秀娟, 赵国瑞, 董东东, 等. 选区激光熔化制造 Inconel625 高温合金的组织及力学性能[J]. 中国激光, 2019, 46(12): 1202002.
- [6] Zhu Y Y, Chen B, Tang H B, et al. Influence of heat treatments on microstructure and mechanical properties of laser additive manufacturing Ti-5Al-2Sn-2Zr-4Mo-4Cr titanium alloy[J]. Transactions of Nonferrous Metals Society of China, 2018, 28(1): 36-46.
- [7] Zhang J L, Li F L, Zhang H J. Research progress on preparation of metallic materials by selective laser melting [J]. Laser & Optoelectronics Progress, 2019, 56(10): 100003.
- 张家莲, 李发亮, 张海军. 选区激光熔化技术制备金属材料研究进展[J]. 激光与光电子学进展, 2019, 56(10): 100003.
- [8] Zhou Q J, Yan Z Y, Han X, et al. Microstructure and mechanical properties of laser melting deposited TC11 titanium alloys[J]. Chinese Journal of Lasers, 2018, 45(11): 1102005.
- 周庆军, 严振宇, 韩旭, 等. 激光熔化沉积 TC11 钛合金的组织与力学性能[J]. 中国激光, 2018, 45 (11): 1102005.
- [9] Zhu Y Y, Liu D, Tian X J, et al. Characterization of microstructure and mechanical properties of laser melting deposited Ti-6.5Al-3.5Mo-1.5Zr-0.3Si titanium alloy [J]. Materials & Design, 2014, 56: 445-453.
- [10] Liu Z, Qin Z X, Liu F, et al. The microstructure and mechanical behaviors of the Ti-6.5Al-3.5Mo-1.5Zr-0.3Si alloy produced by laser melting deposition[J]. Materials Characterization, 2014, 97: 132-139.
- [11] Gu D D, Zhang H M, Chen H Y, et al. Laser additive manufacturing of high-performance metallic aerospace components[J]. Chinese Journal of Lasers, 2020, 47(5): 0500002.
- 顾冬冬, 张红梅, 陈洪宇, 等. 航空航天高性能金属材料构件激光增材制造[J]. 中国激光, 2020, 47 (5): 0500002.
- [12] Jing G Y, Wei K W, Wang Z M, et al. Microstructure and mechanical property of S-04 steel by selective laser melting [J]. Laser & Optoelectronics Progress, 2016, 53(11): 111404.
- 靖冠乙, 魏恺文, 王泽敏, 等. 激光选区熔化成形 S-04 钢的组织及性能[J]. 激光与光电子学进展, 2016, 53(11): 111404.
- [13] Zheng Y L, He Y L, Chen X H, et al. Elevated-temperature tensile properties and fracture behavior of GH3536 alloy formed via selective laser melting [J]. Chinese Journal of Lasers, 2020, 47 (8): 0802008.
- 郑寅岚, 何艳丽, 陈晓晖, 等. 选区激光熔化成形 GH3536 合金的高温拉伸性能及断裂行为分析[J]. 中国激光, 2020, 47(8): 0802008.
- [14] Xiao Z N, Liu T T, Liao W H, et al. Microstructure and mechanical properties of TC4 titanium alloy formed by selective laser melting after heat treatment [J]. Chinese Journal of Lasers, 2017, 44 (9): 0902001.
- 肖振楠, 刘婷婷, 廖文和, 等. 激光选区熔化成形 TC4 钛合金热处理后微观组织和力学性能[J]. 中国激光, 2017, 44(9): 0902001.
- [15] Zhang W X, Tang C L, Chen Z R, et al. Effect of annealing temperature on microstructure and mechanical properties of TC4 titanium alloy formed by selective laser melting [J]. Heat Treatment of Metals, 2019, 44(6): 122-127.
- 张伟祥, 唐超兰, 陈志茹, 等. 退火温度对激光选区熔化成形 TC4 钛合金组织及力学性能的影响[J]. 金属热处理, 2019, 44(6): 122-127.
- [16] Vrancken B, Thijs L, Kruth J P, et al. Heat treatment of Ti₆Al₄V produced by selective laser melting: microstructure and mechanical properties [J]. Journal of Alloys and Compounds, 2012, 541: 177-185.
- [17] Yang J J, Yu H C, Yin J, et al. Formation and control of martensite in Ti-6Al-4V alloy produced by selective laser melting [J]. Materials & Design, 2016, 108: 308-318.
- [18] Calderon-Moreno J M, Vasilescu C, Drob S I, et al. Microstructural and mechanical properties, surface and electrochemical characterisation of a new Ti-Zr-Nb alloy for implant applications [J]. Journal of Alloys and Compounds, 2014, 612: 398-410.
- [19] Liang X K, Dong P, Chen J L, et al. Microstructure and mechanical properties of selective laser melting Ti-6Al-4V alloy [J]. Applied Laser, 2014, 34(2): 101-104.
- 梁晓康, 董鹏, 陈济轮, 等. 激光选区熔化成形 Ti-6Al-4V 钛合金的显微组织及性能[J]. 应用激光, 2014, 34(2): 101-104.
- [20] Yang G, Wang W D, Qin L Y, et al. Effect of annealing temperature and soaking time on microstructures and microhardness of laser deposition manufacturing TA15 titanium alloy [J]. Infrared and Laser Engineering, 2017, 46(8): 0806006.
- 杨光, 王文东, 钦兰云, 等. 退火温度及保温时间对激光沉积制造 TA15 钛合金微观组织和显微硬度的影响[J]. 红外与激光工程, 2017, 46(8): 0806006.

- [21] Yin J, Peng G Y, Chen C P, et al. Thermal behavior and grain growth orientation during selective laser melting of Ti-6Al-4V alloy [J]. *Journal of Materials Processing Technology*, 2018, 260: 57-65.
- [22] Yang J J, Han J, Yu H C, et al. Role of molten pool mode on formability, microstructure and mechanical properties of selective laser melted Ti-6Al-4V alloy [J]. *Materials & Design*, 2016, 110 (15): 558-570.
- [23] Angelier C, Bein S, Béchet J. Building a continuous cooling transformation diagram of β -CEZ alloy by metallography and electrical resistivity measurements [J]. *Metallurgical and Materials Transactions A*, 1997, 28(12): 2467-2475.
- [24] Qin L Y, Xu L L, Yang G, et al. Effect of annealing method on microstructure and mechanical properties of TA15 titanium alloys by laser deposition manufacturing [J]. *Chinese Journal of Lasers*, 2018, 45(3): 0302004.
- 钦兰云, 徐丽丽, 杨光, 等. 退火方式对激光沉积 TA15 钛合金组织及力学性能的影响 [J]. *中国激光*, 2018, 45(3): 0302004.

Effect of Heat Treatment on Microstructure and Mechanical Properties of Selective-Laser-Melted TC11 Titanium Alloys

Dou Enhui*, Xiao Meili, Ke Linda, Du Lei, Lai Caifang
Shanghai Spaceflight Precision Machinery Institute, Shanghai 201600, China

Abstract

Objective Selective laser melting (SLM), because of its capacity to fabricate complex precision parts with high forming accuracy, has been hailed as one of the most promising manufacturing technologies for rapid prototyping. However, the mechanical properties of metal materials formed by SLM have the characteristics of anisotropy, high strength, and low plasticity. Therefore, heat treatment is always needed to control the microstructure to meet application requirements. Annealing treatment is typically adopted to improve the mechanical properties of selective-laser-melted titanium alloys. Therefore, study of the effect of annealing temperature and holding time on the microstructure, mechanical properties, and fracture mechanism of TC11 titanium alloys formed by SLM is of great significance.

Methods The resulting microstructure, mechanical properties, and fracture morphology of selective-laser-melted TC11 titanium alloys under different heating temperature and holding time were studied, and the fracture mechanism under different conditions was explored. Firstly, compact TC11 titanium alloys were obtained by SLM. Secondly, different annealing heat treatments were performed on the samples. Thirdly, the phase composition of the different samples was analyzed by X-ray diffraction, and the microstructure morphology was observed by optical microscopy (OM) and scanning electron microscopy (SEM). Finally, the change in the micro-hardness of different samples was tested using a micro-hardness tester, the tensile properties at room temperature were tested, and the fracture morphology was observed by SEM.

Results and Discussions The as-deposited TC11 titanium alloys are composed of hexagonal close-packed Ti (HCP/Ti), with lattice parameters a and c of 0.2934 nm and 0.46757 nm, respectively. The annealed samples consisted of HCP/Ti and body center cubic Ti (BCC/Ti), where a and c for HCP/Ti are 0.29172 nm and 0.46817 nm, respectively (Fig. 3). Based on the observation of microstructure morphology by OM and SEM, it is deduced that the selective-laser-melted TC11 titanium alloys consisted of columnar grains, within which acicular α' martensite was present (Fig. 4). After annealing at 850 °C for 4 h, fine $\alpha + \beta$ mixed structures were formed in the alloys, this was the result of the nucleation and growth of α' martensite. Due to the sufficient atomic diffusion leading to coarsening α lamellae, basket-weave structures were formed in the samples annealed at 950 °C for 4 h. Moreover, α clusters with the same orientation and continuous grain boundary α phase (GB α) were also observed in the grains and at the grain boundaries, respectively (Fig. 5). When annealing temperature remained at 950 °C with holding time of 1 h or 2 h, basket-weave structures were also formed in the samples, but the width of α lamellae was about one-half and one-quarter of that in the samples annealed at 950 °C for 4 h, respectively. In addition, GB α phase began to transform into a discontinuous distribution (Fig. 6). According to the results of the hardness test, the average micro-hardness of the as-deposited samples is about 402 HV_{0.5}, whereas the hardness of the samples annealed at 950 °C for

4 h is only about 85% that of the as-deposited samples. Moreover, the micro-hardness of the samples annealed at the same temperature for 2 h and 1 h is about 381 HV_{0.5} and 393 HV_{0.5}, respectively. The increase in micro-hardness with the decrease in holding time could be due to the effect of fine-grained strengthening (Fig. 7). The tensile strength and percentage elongation after fracture is 1557 MPa and 2.5%, respectively, because acicular martensite is characterized by high strength and poor plasticity. However, after the samples were annealed at 850 °C and 950 °C for 4 h, the tensile strength is 72% and 64% of that of the as-deposited samples, respectively. In this case, the percentage elongation after fracture is 4.5 times and 5.7 times that of the as-deposited samples, respectively. When the samples were annealed at 950 °C, their tensile strength increased from 996 to 1051 MPa, and the percentage elongation after fracture increased from 14.3% to 19.8% (Fig. 8, Table 3). This is because the fine basket-weave structures have the effect of fine grain strengthening, and GB α has an effect on the percentage elongation after fracture. Based on fracture analysis, no obvious plastic deformation was observed in the macroscopic fracture of the as-deposited samples, and the fracture exhibited granular grain surfaces with different orientations. The microscopic fracture showed the characteristics of intergranular dimples. The above analysis indicates that the as-deposited sample underwent intergranular fracture when it was stretched at room temperature (Fig. 9). However, macroscopic fractures of the annealed state had obvious plastic deformation, and the microscopic fractures showed the characteristics of dimples with larger size, indicating that ductile fracture occurred in the annealed state (Fig. 10).

Conclusions The effect of annealing temperature and holding time on the microstructures, mechanical properties, and fracture mechanism of selective-laser-melted TC11 titanium alloys is investigated, and the following conclusions can be drawn: The microstructures of the alloys are composed of acicular martensite within columnar grains parallel to the building direction. After annealing at 850 °C and 950 °C for 4 h, the microstructures of the alloys are fine $\alpha + \beta$ mixed and $\alpha + \beta$ basket-weave structures, respectively. As a result of decomposition of the acicular martensite, the alloys are softened, and the softening effect is more obvious with the increase in annealing time or temperature. Furthermore, the fracture mechanism changes from being intergranular to ductile, which is consistent with the regular variation of the percentage elongation after fracture. When the alloys are annealed at 950 °C, with shorter holding time, finer lamellar α can be obtained. Continuous GB α transforms into a discontinuous distribution, finally resulting in the simultaneous increase in tensile strength and elongation after fracture. Selective-laser-melted TC11 titanium alloys with better strength and plasticity can be obtained through annealing at 950 °C for 1 h, with a tensile strength and percentage elongation of 1051 MPa and 19.8%, respectively, after fracture.

Key words laser technique; selective-laser-melting; TC11 titanium alloy; heat treatment; microstructure and mechanical property; fracture mechanism

OCIS codes 140.3390; 160.3900; 350.3850